

FPGA-based phase control of acousto-optic modulator Fourier synthesis system through gradient descent phase-locking algorithm

KENNETH J. UNDERWOOD,^{1,*} ANDREW M. JONES,² AND JULIET T. GOPINATH²

¹University of Colorado Boulder, Department of Physics, Boulder, Colorado 80309, USA

²University of Colorado Boulder, Department of Electrical, Computer and Energy Engineering, Boulder, Colorado 80309, USA

*Corresponding author: kenneth.underwood@colorado.edu

Received 16 March 2015; revised 19 May 2015; accepted 19 May 2015; posted 26 May 2015 (Doc. ID 236218); published 12 June 2015

We present a new application of the stochastic parallel gradient descent (SPGD) algorithm to fast active phase control in a Fourier synthesis system. Pulses (4.9 ns) with an 80 MHz repetition rate are generated by feedback from a single phase-sensitive metric. Phase control is applied via fast current modulation of a tapered amplifier using an SPGD algorithm realized on a field-programmable gate array (FPGA). The waveforms are maintained by constant active feedback from the FPGA. We also discuss the extension of this technique to many more semiconductor laser emitters in a diode laser array. © 2015 Optical Society of America

OCIS codes: (140.3298) Laser beam combining; (140.2020) Diode lasers; (140.3538) Lasers, pulsed.

<http://dx.doi.org/10.1364/AO.54.005624>

1. INTRODUCTION

Active phase control techniques have found application in many facets of adaptive optics, ranging from atmospheric wavefront compensation for astronomical images to coherent beam combining systems for maximizing the power output of both cw and pulsed laser arrays. Use of the stochastic parallel gradient descent (SPGD) algorithm has been instrumental in the growth of adaptive optics due to its efficiency, model-free optimization performance, stable operation from a single system performance metric, and strong scalability to large numbers of elements [1,2]. Adaptive wavefront correction using SPGD with over 100 channels has been demonstrated on a variety of wavefront correctors, including deformable mirrors [3] and micromechanical mirror systems [4]. Still higher resolution wavefront correction has been achieved using phase-correcting liquid crystal spatial light modulators using Zernike polynomials as influence functions [5]. Combined beam steering and adaptive wavefront correction projects using SPGD for laser weapons and sensing systems are also in development [6].

In coherent beam combining systems, the SPGD algorithm has corrected piston phase drifts for up to 218 different laser elements [2] and consistently demonstrated highly scalable phase control with high coherence through a number of experimental metrics [2,7,8]. The technique has been applied to diode lasers as well as fiber lasers and fiber amplifiers, generating as much as 4 kW from an SPGD-combined fiber amplifier array with 78% combining efficiency [8]. These results, while impressive, have been limited to combining laser elements at

the same frequency, optimizing a spatial intensity profile to generate high-power cw output or improved beam quality. In this paper we report on the application of the SPGD algorithm to a phase control system in a Fourier synthesis architecture, where active phase control is instead used to generate pulses from frequency-separated cw light.

In the same way that optical pulses are analyzed by being broken down into their constituent sine-wave frequencies (Fourier analysis), these same sine-waves can be combined together in-phase to instead generate the original pulses (Fourier synthesis). The Fourier synthesis technique is particularly attractive for time-resolved measurements and optical communication due to its direct control over both repetition rate and pulse width within the system time-bandwidth product. Optical pulse generation by Fourier synthesis was first demonstrated in 1977 [9], but was limited in scale by the necessity for individual detectors for every emitter. Semiconductor lasers were first used for pulse synthesis by Mukai *et al.* [10] using a nonlinear phase-locking process, but again lacked scalability, as each additional emitter required an additional nonlinear crystal and optical phase-locked loop (OPLL) system [11]. Experiments by Futami and Kikuchi [12], and Hyodo *et al.* [13] generating phase-locked frequencies through four-wave mixing had similar issues with extending the technique.

Here we report on a direct-diode phase control system using a single linear phase-sensitive metric, controlled though an SPGD algorithm implemented on a field-programmable gate array (FPGA) controller. This technique uses a narrow-linewidth

source separated by acousto-optic modulators (AOMs) into three cw beams and Fourier combined into a stable 80 MHz pulse train. The waveform of the pulse train is maintained over a prolonged period by fast active feedback from an FPGA controller receiving cost function data from the single linear phase-sensitive metric. It should be noted that although here we apply the SPGD algorithm to the control of only one element, many experiments have demonstrated straightforward scaling of the SPGD phase control system to multiple elements in a variety of systems. The primary improvement enabled by the FPGA with the SPGD algorithm is the ability to perform multiple locks with a single performance metric. In contrast, an OPLL scheme would require a detector and servo filter for each additional emitter. We focus on one element here solely as a proof-of-concept, not due to a restriction of the Fourier synthesis phase control strategy. Phase control of light at different frequencies represents a new application space for active feedback using the SPGD algorithm.

While this approach only addresses the phase control aspects of such a pulse generation system, a more scalable frequency separation technique is currently being developed which will also be applicable to lasers from which it has been traditionally difficult to obtain pulsed output, such as quantum cascade lasers. This approach makes use of a diode laser array in a frequency-selective external cavity to set the frequency separation, along with a stable, high finesse cavity and EOM-based optical comb generator as a reference, with frequency locking through active SPGD stabilization of emission lines to cavity transmission resonances. Such a frequency separation system is scalable with minor alterations for many more elements, but is beyond the scope of this paper. Our research lays the groundwork for such a system by demonstrating effective single-element phase control of a multifrequency system through model-free optimization with a fast FPGA controller.

2. EXPERIMENTAL SETUP

The beam combining experimental setup is shown in Fig. 1. A single-mode antireflection-coated 780 nm laser diode in Littrow configuration, the “master laser,” is coupled into a 1 W GaAs tapered amplifier (TA). With minimal temperature and mechanical stabilization the master laser has a linewidth of ~1 MHz and cw output power of 25 mW. Amplified light out of the first TA (TA1) encounters a polarizing beam cube, where one arm is split off to seed a second tapered amplifier of the same model. Where the first tapered amplifier is used to

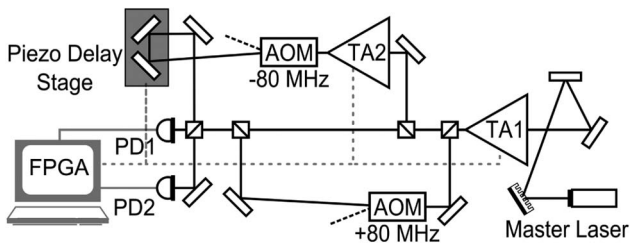


Fig. 1. Experimental setup for Fourier synthesis system: AOM, acousto-optic modulator; TA1, TA2, tapered amplifiers; PD1, PD2, photodetectors; FPGA, field-programmable gate array.

provide enough power to downstream components to ensure usable signal-to-noise ratio, the second TA provides both optical gain and a controllable current-modulated phase shift through thermal variation of the refractive index of the tapered amplifier chip [14]. Spatial variations in the beams are considered to be stable over the time scales involved, contributing minimally to the observed phase excursions. After this amplification/phase-control stage, the single-frequency light passes through two acousto-optic modulators (Gooch and Housego model R23080-2-LTD) [15], which shift the light into three beams separated in frequency by 80 MHz, forming f_0 , $f_1 = f_0 - 80$ MHz, and $f_2 = f_0 + 80$ MHz. The phase of frequency f_1 is then controlled again by a piezo-driven delay stage before being superimposed on a common optical axis with the other two beams, forming the pulse train. The characteristics of the Fourier synthesized waveform are determined using a series of Si photodetectors.

Due to the amplitude-sensitive phase locking requirements of the FPGA controller algorithm and the high operating frequency of the AOM driver compared to the FPGA clock frequency (50 MHz), two detection signals must be provided to the FPGA; the first provides the peak power and the second the average power. In order to determine the peak power, the maximum of the combined output is measured by half-wave rectification of an AC-coupled 1 GHz photodiode signal, forming a phase-dependent signal with a bandwidth of 160 kHz. Specifically, the rectified photodetector response is given by a maximum of the field intensity,

$$I(t, \theta) = A_0^2 |e^{i(\omega+\omega_0)t} + e^{i(\omega-\omega_0)t+\theta} + e^{i\omega t}|^2, \quad (1)$$

with field amplitude A_0 , center frequency $\omega = 2\pi f_0$, frequency shift $\omega_0 = 2\pi \times 80$ MHz, and phase shift θ . Simplifying this equation results in

$$I(t, \theta) = 2A_0^2 \left(\frac{3}{2} + \cos \omega t + \cos(\omega t - \theta) + \cos(2\omega t - \theta) \right), \quad (2)$$

which has its maximum intensity at $t = 2\pi n/\omega$ for $n = 0, 1, 2, \dots$, where

$$I(2\pi n/\omega, \theta) = A_0^2 (5 + 4 \cos \theta). \quad (3)$$

This low-frequency phase-dependent signal, which is directly proportional to the peak power, can then be read by the FPGA controller, where it is normalized to the range 0 to 1 and provides the cost function $J = (1 + \cos \theta)/2$ to be optimized with the SPGD algorithm. While this electronic fast-photodiode phase-dependent measurement system is appropriate for the 160 MHz bandwidth demonstrated here, wider bandwidth operation can be enabled through the use of a balanced autocorrelation scheme to form the cost function instead. The second detector measures the total average power of the combined beam with a 1.9 MHz bandwidth, passing this information to the FPGA controller as well. This experiment was not optimized for power combining efficiency [2,8], but rather for balanced overlap of individual beams. The measured combining efficiency of ~30% could be improved with more careful engineering of the optical system. A third detector with a >1.2 GHz bandwidth provides fast direct waveform measurement monitored on a 1 GHz oscilloscope, not shown in the figure. This data is used for diagnostic purposes only.

To stabilize the phase and amplitude of the generated pulses, we use a dedicated FPGA with a threefold control mechanism. We implement the necessary active phase control through an SPGD algorithm, shown to provide robust control in many facets of adaptive optics [3,5]. A slow, large amplitude SPGD algorithm applied to a piezo-driven delay stage at 80 Hz corrects for large slow fluctuations (0–40 Hz) in the phase between the three beams as measured by our cost function above. A faster smaller amplitude SPGD algorithm is applied instead to the drive current of TA2, operating at 12 kHz, to correct for smaller fast fluctuations (40–6000 Hz) in the phase.

The stochastic parallel gradient descent algorithm [3,16,17] in its most general form is

$$u^{(n+1)} = u^{(n)} - \gamma(\delta J / \delta u), \quad (4)$$

where u is the controller output, n the iteration number, δu the small random perturbation in the control output, δJ the resultant small change in the cost function, and the weighting parameter γ [16]. With random perturbations, the expectation value of the stochastic vector $\delta J / \delta u$ approximates the true gradient of J . Jumps along that approximate gradient therefore iteratively optimize the cost function.

We implement the SPGD algorithm for slow feedback to the piezo and faster feedback to the tapered amplifier. In the slow SPGD algorithm, u designates the piezo voltage, while u in the fast algorithm denotes the TA current. In both cases, the cost function J is given by the phase-dependent detector signal. The magnitude of the weighting parameter γ adapts with the proximity of the system to the extrema of the cost function, with γ increasing in strength as the cost function diverges from the ideal. This “adaptive” active control is designed to increase the convergence rate while minimizing the standard deviation of the cost function as described in [18]. With more elements, the only algorithmic change is a shift from single values to arrays of the relevant parameters. The same single cost function is used.

As the TA phase correction current adjustments also slightly alter the power emitted by the second TA, fast corrections to the total power (40 kHz) are made to the first TA to reduce the effect of this power-current relationship. These corrections are made using a tuned proportional-integral-derivative (PID) feedback loop controller also realized on the FPGA, where the gain coefficients of the PID loop were arrived at through standard Ziegler–Nichols tuning [19]. The 0.1 MHz AC-coupling in PD1 also acts to decrease the impact of total power fluctuations in the phase-dependent signal, though does not remove them entirely due to the nonlinear relationship of the average input power to the peak intensity signal from the half-wave rectifier.

3. EXPERIMENTAL RESULTS AND DISCUSSION

Synthesized waveforms given in Fig. 2 show in-phase and out-of-phase operation at a frequency separation of 80 MHz. Theoretical curves for the waveforms given in Eq. (2) are also included, with phase separation $\theta = 0, \pi$. The RF spectrum of the fundamental in Fig. 3 demonstrates the >20 dB discrimination between in-phase and out-of-phase peaks, indicating the sufficiently balanced power between the three arms. These

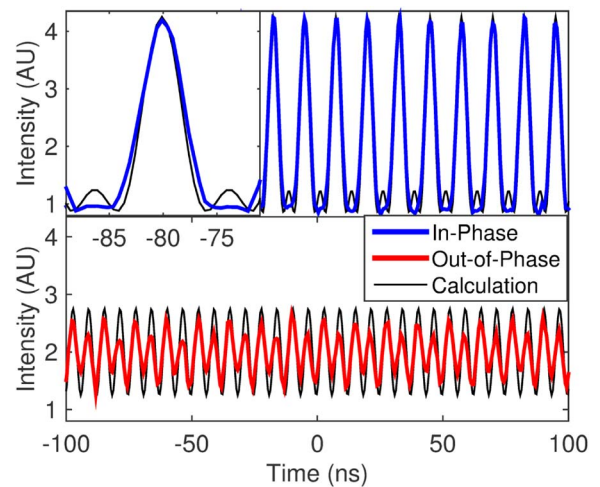


Fig. 2. Synthesized waveforms from Fourier combined beams with single pulse inset. In-phase corresponds to $\Delta\phi = 0$, where $\Delta\phi$ describes the phase difference between the beat note $f_0 - f_1$ and the beat note $f_0 - f_2$. Out-of-phase refers to $\Delta\phi = \pi$. Deviations of the experimental results from calculated waveforms are primarily due to power imbalances between beams.

signals are amplified for peak discrimination using a 25 dB gain low-noise RF amplifier (ZFL-1000LN+, 2.9 dB noise figure) [15]. Analysis of this amplitude noise spectrum using a Von der Linde approach [20] in the noise burst model gives the width of the noise envelope at 5 kHz, corresponding to 8% intrinsic energy fluctuations in the pulses. These fluctuations can be explained completely by the 5 kHz linewidth of the RF driving frequency for the acousto-optic modulator.

The phase noise spectral density (PNSD) of the system is shown in Fig. 4. By splitting off the AOM driver frequency and mixing it with the 80 MHz photodiode signal in an IQ mixer architecture we were able to measure the phase noise from 1 Hz up to 1 MHz in the tapered amplifier-piezo delay stage (TA2, PDS) arm, the frequency separation arm with only passive optical media (mirrors, beam splitters), and the AOM drive signal itself to act as a noise baseline [21]. Data was recorded at 1 MS/s over 20 s using a Tektronix MDO 4104B-6 oscilloscope [15], where the PNSD was approximated

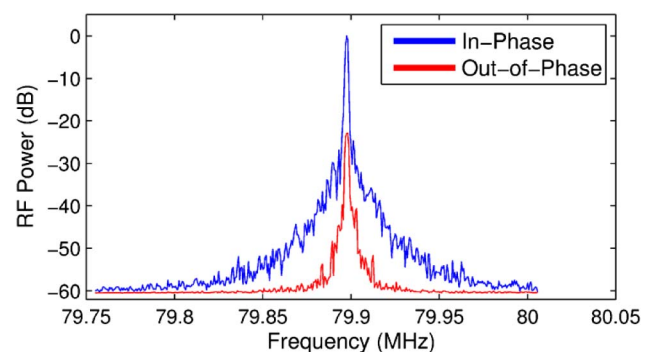


Fig. 3. RF beat note spectrum for $\Delta\phi = 0$ (in-phase) and π (out-of-phase). Note large 20 dB discrimination between in-phase and out-of-phase peaks as well as narrow linewidth noise envelope given by radio-frequency driver for acousto-optic modulators.

with a periodogram smoothed to reduce measurement noise. This PNSD measurement of the individual arms of the Fourier synthesis system is analogous to a phase-noise analysis of an actively mode-locked diode laser.

In Fig. 4, the phase noise present in the primary control arm (TA2, PDS) is compared with the noise in the arm which interacts with only mirrors as well as the bare drive signal to the AOM. The majority of phase noise activity is present at low (~0–40 Hz) and medium operating frequencies (40–6000 Hz), as indicated by the dashed lines in Fig. 4. Low-frequency terms are present in both of the measured beams, while stronger mid-range peaks can be seen in the TA2, PDS spectral density. This suggests that low-frequency phase noise is primarily a result of thermal and mechanical effects in the mirrors present in both arms as well as free space eddies, and 100–1000 Hz phase noise originates primarily in the tapered amplifier. The vertical dashed lines in the figure demonstrate the motivation for the operating bandwidth of the piezo delay stage and tapered amplifier controllers. The 80 Hz PDS encompasses most large slow fluctuations, and the 12 kHz TA controller handles medium strength, mid-frequency-range phase noise. This 12 kHz maximum operating speed is in no way restricted by the operating rate of the FPGA system used, which can reach 780 kHz with the possibility for more advanced systems to extend to the gigahertz range. The relatively slow operating regime here was selected to be the minimum speed required to encompass the majority of the noise, as shown in Fig. 4, while maximizing the amount of FPGA signal averaging available to reduce measurement noise.

Figure 5 demonstrates the effectiveness of the control system on the normalized cost function (representing the peak power of the synthesized waveform) in open-loop and closed-loop states over different time scales, over 4.7 s [Fig. 5(a)] and over 5 min [Fig. 5(b)], monitored by the FPGA at 40 kHz. Slow, <40 Hz variations in the phase are due to thermal effects, with ~200 Hz phase excursions arising from mechanical vibrations of optical components in the beam path such as mirrors and lenses. Still higher-frequency phase excursions (>10 kHz) are the result of minor instabilities in the single-frequency nature

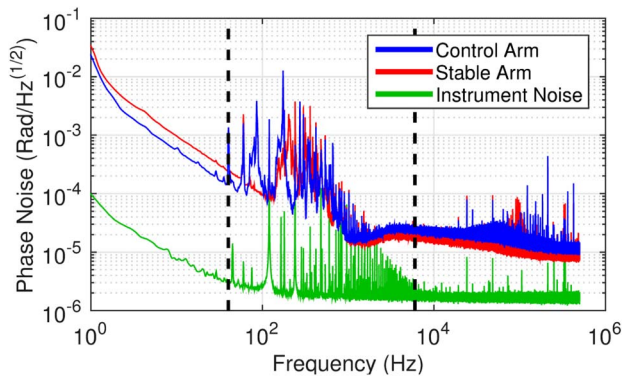


Fig. 4. TA2, tapered amplifier in phase control arm; PDS, piezo delay stage. Phase noise spectral density of Fourier synthesis system, with phase noise of control arm (TA2, PDS) compared to phase noise of mirror arm and instrument noise floor. Vertical dashed lines show bandwidth of slow (40 Hz) piezo controller and fast (6 kHz) TA controller.

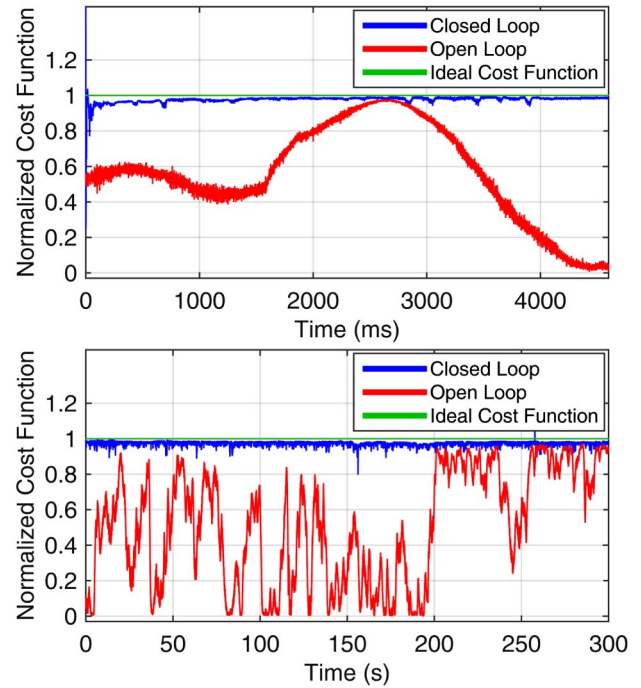


Fig. 5. FPGA phase control system performance (a) over 4.7 s and (b) over 5 min. When the system is in a closed-loop state with FPGA control on, the normalized cost function stays close to one and shows minimal phase deviation. In contrast, large phase fluctuations are seen when the system is in open loop, i.e., FPGA control off.

of the master laser. When these phase fluctuations of different components are not being controlled, the system is in open loop and the cost function fluctuates randomly. Alternatively, when phase fluctuations of different components are being controlled and the system is in a closed-loop state, the cost function normalized to its experimentally derived maximum stays close to one. For a completely uncontrolled system, the standard deviation of the cost function (proportional to the cosine of the phase as $J = (1 + \cos \theta)/2$) approaches $\sigma = 1/2\sqrt{2}$, or ~0.353. This value is close to the measured open-loop standard deviation of 0.33. In the closed-loop state, the standard deviation of the cost function improves by over an order of magnitude to 0.032, with remaining deviations arising from the SPGD dither.

4. CONCLUSIONS

We have experimentally demonstrated the application of an SPGD-based active phase control system to an optical pulse train generator based on the Fourier synthesis of AOM-separated light obtained from an amplified narrow-linewidth cw semiconductor seed laser. We controlled the amplitude and phase of one frequency component using an SPGD implemented on a dedicated FPGA board, and successfully generated a pulse train with an 80 MHz repetition rate and 4.9 ns pulse width with an order of magnitude improvement in phase stability. With a suitable frequency separation system, the transition to an array of independent cw lasers would allow for straightforward scaling of the phase control system, with phase noise limited by the bandwidth of the FPGA feedback.

Air Force Office of Scientific Research (AFOSR) (FA9550-11-1-0026).

The authors gratefully acknowledge technical contributions from David Glugla and equipment loans from Tektronix, Inc.

REFERENCES AND NOTES

1. M. Vorontsov and V. Sivokon, "Stochastic parallel-gradient-descent technique for high-resolution wave-front phase-distortion correction," *J. Opt. Soc. Am. A* **15**, 2745–2758 (1998).
2. S. Redmond, K. Creedon, J. Kinsky, S. Augst, L. Missaggia, M. Connors, R. Huang, B. Chann, T. Fan, G. Turner, and A. Sanchez-Rubio, "Active coherent beam combining of diode lasers," *Opt. Lett.* **36**, 999–1001 (2011).
3. T. Weyrauch and M. Vorontsov, "Dynamic wave-front distortion compensation with a 134-control-channel submillisecond adaptive system," *Opt. Lett.* **27**, 751–753 (2002).
4. B. Dong, D. Ren, and X. Zhang, "Stochastic parallel gradient descent based adaptive optics used for a high contrast imaging coronagraph," *Res. Astron. Astrophys.* **11**, 997–1002 (2011).
5. H. Ma, Z. Liu, X. Xu, S. Wang, and C. Liu, "Near-diffraction-limited flat-top laser beam adaptively generated by stochastic parallel gradient descent algorithm," *Opt. Lett.* **35**, 2973–2975 (2010).
6. T. Dorschner, "Adaptive photonic phase locked elements: an overview," Raytheon Network Centric Systems presentation (2007).
7. P. Zhou, Z. Liu, X. Wang, Y. Ma, H. Ma, X. Xu, and S. Guo, "Coherent beam combining of fiber amplifiers using stochastic parallel gradient descent algorithm and its application," *IEEE J. Sel. Top. Quantum Electron.* **15**, 248–256 (2009).
8. C. Yu, S. Augst, S. Redmond, K. Goldizen, D. Murphy, A. Sanchez, and T. Fan, "Coherent combining of a 4 kW, eight-element fiber amplifier array," *Opt. Lett.* **36**, 2686–2688 (2011).
9. C. Hayes and L. Laughman, "Generation of coherent optical pulses," *Appl. Opt.* **16**, 263–264 (1977).
10. T. Mukai, R. Wynands, and T. Hänsch, "Optical pulse synthesis with three cw semiconductor lasers using nonlinear phase-locking," *Opt. Commun.* **95**, 71–76 (1993).
11. N. Satyan, W. Liang, A. Kewitsch, G. Rakuljic, and A. Yariv, "Phase locking of semiconductor lasers using homodyne detection and negative electrical feedback," *IEEE J. Sel. Top. Quantum Electron.* **15**, 240–247 (2009).
12. F. Futami and K. Kikuchi, "Generation of 113-GHz, 1.8-ps optical pulse trains by Fourier synthesis of four-wave mixing signals obtained from semiconductor optical amplifiers," *Opt. Lett.* **22**, 1873–1875 (1997).
13. M. Hyodo, N. Onodera, and K. Abedin, "Fourier synthesis of 9.6-GHz optical-pulse trains by phase locking of three continuous-wave semiconductor lasers," *Opt. Lett.* **24**, 303–305 (1999).
14. M. Fukuda, T. Mishima, N. Nakayama, and T. Masuda, "Temperature and current coefficients of lasing wavelength in tunable diode laser spectroscopy," *Appl. Phys. B* **100**, 377–382 (2010).
15. Mention of commercial products is for information only; it does not imply endorsement or recommendation.
16. M. Vorontsov, G. Carhart, and J. Ricklin, "Adaptive phase-distortion correction based on parallel gradient-descent optimization," *Opt. Lett.* **22**, 907–909 (1997).
17. R. Su, P. Zhou, X. Wang, Y. Ma, and X. Xu, "Active coherent beam combination of two high-power single-frequency nanosecond fiber amplifiers," *Opt. Lett.* **37**, 497–499 (2012).
18. T. Weyrauch, M. Vorontsov, T. Bifano, J. Hammer, M. Cohen, and G. Cauwenberghs, "Microscale adaptive optics: wave-front control with a μ -mirror array and a VLSI stochastic gradient descent controller," *Appl. Opt.* **40**, 4243–4253 (2001).
19. J. Ziegler and N. Nichols, "Optimum settings for automatic controllers," *Trans. ASME* **64**, 759–768 (1942).
20. D. von der Linde, "Characterization of the noise in continuously operating mode-locked lasers," *Appl. Phys. B* **39**, 201–217 (1986).
21. S. Augst, T. Fan, and A. Sanchez, "Coherent beam combining and phase noise measurements of ytterbium fiber amplifiers," *Opt. Lett.* **29**, 474–476 (2004).